Evidence for Flat Bands near the Fermi Level in Epitaxial Rhombohedral Multilayer Graphene

Debora Pierucci,[†] Haikel Sediri,[†] Mahdi Hajlaoui,[†,‡] Jean-Christophe Girard,[†] Thomas Brumme,[§] Matteo Calandra,[*,§] Emilio Velez-Fort,[†,§] Gilles Patriarche,[†] Mathieu G. Silly,[‡] Gabriel Ferro,[∥] Véronique Soulière,[∥] Massimiliano Marangolo,[⊥,#] Fausto Sirotti,[‡] Francesco Mauri,[*,§] and Abdelkarim Ouerghi[*,†]

[†]Laboratoire de Photonique et de Nanostructures (CNRS-LPN), Route de Nozay, 91460 Marcoussis, France, [‡]Synchrotron-SOLEIL, Saint-Aubin, BP48, F91192 Cedex Gif sur Yvette, France, [§]Institut de Minéralogie, de Physique des Matériaux, et de Cosmochimie, UMR CNRS 7590, Sorbonne Universités, UPMC, Univ. Paris VI, MNHN, IRD, 4 place Jussieu, 75005 Paris, France, [∥]Laboratoire des multimateriaux et Interfaces, UMR 5615, Université Claude Bernard Lyon I, 69100 Villeurbanne, France, [⊥]UMR 7588, INSP, Sorbonne Universités, UPMC Univ Paris 06, 4 place Jussieu, F-75005 Paris, France, and [#]CNRS, UMR 7588, Institut des Nanosciences de Paris, 4 place Jussieu, F-75005 Paris, France

ABSTRACT The stacking order of multilayer graphene has a profound influence on its electronic properties. In particular, it has been predicted that a rhombohedral stacking sequence displays a very flat conducting surface state: the longer the sequence, the flatter the band. In such a flat band, the role of electron−electron correlation is enhanced, possibly resulting in high T_c superconductivity, magnetic order, or charge density wave order. Here we demonstrate that rhombohedral multilayers are easily obtained by epitaxial growth on 3C-SiC(111) on a 2° off-axis 6H-SiC(0001). The resulting samples contain rhombohedral sequences of five layers on 70% of the surface. We confirm the presence of the flat band at the Fermi level by scanning tunneling spectroscopy and angle-resolved photoemission spectroscopy, in close agreement with the predictions of density functional theory calculations.

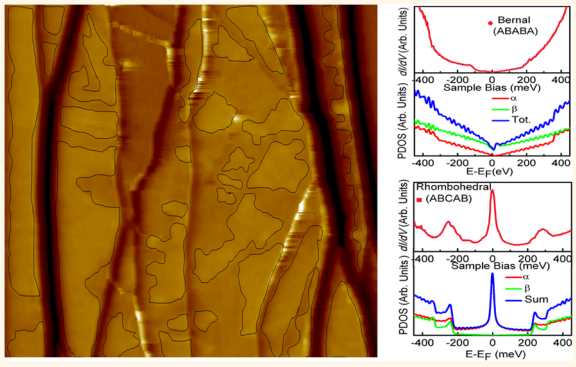

KEYWORDS: rhombohedral multilayer graphene · flat band · density functional theory · angle-resolved photoemission spectroscopy · STM/STS · STEM

Flat band materials are one promising route in the century-long search for room temperature superconductors or exotic magnetic and/or charge orders.[1] Among the materials under investigation, rhombohedral graphite is predicted to feature a topologically protected surface state with a nearly dispersionless electron excitation spectrum near the Fermi level (flat band) that, because of electron−electron interaction, is prone to superconducting and magnetic instabilities.[2,3] The flatness and the extension in reciprocal space of such flat band increase with the number of subsequent layers with rhombohedral (ABC) stacking.[2,3] Locally ordered rhombohedral sequences are found in natural graphite as defects of the more thermodynamically stable Bernal (AB) stacking.[4−7] Concerning graphene, the main route to get the ABC stacking is the epitaxial approach, based on SiC substrate graphitization.

In this context, prior to the graphitization process, it is important to choose appropriately the SiC polytype. Norimatsu *et al.*[4] chose hexagonal 6H- and 4H-SiC and performed STEM (scanning transmission electron microscopy) to investigate the presence of rhombohedral stacking in the multilayer graphene. Interestingly, they showed, locally, a coherence length of ABC up to six layers. Nevertheless, no quantification of the total areal density was given. Indeed, hexagonal SiC polytypes are not appropriate to stabilize large ABC domains since the unit cells constitute not fully rhombohedral repeated sequences of SiC bilayers: the ABAB structure of 2H-SiC will favor the Bernal stacking

* Address correspondence to abdelkarim.ouerghi@lpn.cnrs.fr, matteo.calandra@impmc.jussieu.fr, francesco.mauri@impmc.upmc.fr.

Received for review February 25, 2015 and accepted April 20, 2015.

Published online April 20, 2015
10.1021/acsnano.5b01239

of "regular" graphite; the more complex stacking sequences of 6H-SiC (ABCACB) and of 4H-SiC (ABCB) will lead to graphene multilayers mixing Bernal and rhombohedral architectures. On the other hand, a cubic SiC substrate, namely, 3C-SiC(111), provides an ideal template for producing rhombohedral-stacked multilayer graphene with a higher density. Simple crystallographic considerations suggest that rhombohedral multilayer graphene grown on 3C-SiC(111) substrates will be more stabilized than that grown other SiC polytypes. Indeed, the close-packing ABCABC structure along the [111] direction of 3C-SiC offers an ideal scaffolding for rhombohedral graphite. Only a few articles reported the growth of graphene on 3C-SiC-(111) epitaxially grown on low-cost, large-area Si(111) wafers.[8−14] However, stress generation (and thus wafer bowing) is huge, easily leading to cracks inside the SiC layer after only a few micrometer thickness.[15] In addition, the use of Si wafers limits both 3C-SiC and graphene growth processes to those at rather low temperatures (below the Si melting point). In the specific case of graphene, the silicon in the Si substrate starts to evaporate or even melt at the annealing temperatures necessary for conventional UHV graphitization. Consequently, controlled graphene growth is difficult to achieve. A more appropriate way to grow epitaxial graphene would be to work on 3C-SiC(111) epitaxial layers grown on commercial 4H- or 6H-SiC substrates, as shown previously.[16,17] To our knowledge, there is only one work by Coletti *et al.*[17] which focused on trilayer epitaxial graphene on the 3C-SiC-(111)/6H-SiC(0001) substrate using angle-resolved photoemission spectroscopy (ARPES). Their ARPES results suggest that the trilayer graphene exhibits a tendency toward the development of presumably large-area ABC-type stacking. However, such ultrathin films do not permit long ABC sequences and consequently an extended flat band in the reciprocal space. The 3C-SiC(111) substrate can be a good candidate to obtain large-area ABC-stacked graphene, and experimental efforts have to be devoted to obtain long ABC sequences and a dispersionless electron excitation spectrum near the Fermi level. This demands a smart growth procedure to get thick graphene films and a direct visualization of the density and of the length of rhombohedral stacking combined to spectroscopic tools to observe the local density of states and the electronic band structure. The growth of rhombohedral multilayer graphene and a direct visualization of the stacking, the density of rhombohedral stacking, the local density of states, and electronic band structure *via* scanning transmission electron microscopy (STEM), low-temperature scanning tunneling microscopy and spectroscopy (LT-STM/STS), and ARPES have not been reported so far. Clearly, the availability of highly resolved experimental STS and ARPES data for multilayer graphene would allow for a direct comparison with the local density of states and band structure predicted by the density functional theory (DFT), thus leading to a precise determination of the flat band at the Fermi level.

Here we describe the growth of high-density rhombohedral stacking multilayer graphene on 12 μm thick twin-free 3C-SiC(111) grown on 2° off-axis 6H-SiC-(0001). Interestingly, the coherence length of the rhombohedral domains along the axis growth is about five/six layers, permitting the onset of a dispersionless electron excitation spectrum near the Fermi level. In particular, the use of 2° off-axis 6H-SiC seed crystals, and thus of an identically misoriented 3C-SiC(111) epitaxial layer, favors the escape of Si from the increased number of step edges generated by the misorientation and an easier growth of multilayer graphene. Low-energy electron diffraction (LEED) patterns and STEM show unambiguously the epitaxial growth of multilayer graphene. By comparing STM/STS, ARPES measurements, and electronic structure calculations, we unambiguously demonstrate the synthesis of undoped rhombohedral multilayer graphene on 3C-SiC(111) and the occurrence of a flat band at the Fermi level. Our approach represents a significant step toward the scalable synthesis of large-area high-density rhombohedral stacking. Our samples are compatible with the high structural quality and fine thickness control needed to develop graphene-based electronic devices.

RESULTS AND DISCUSSION

The multilayer graphene used in this study was obtained by annealing the substrate at $T = 1600$ °C under atmospheric pressure. Figure 1a shows LEED patterns of a probed area of approximately 1 mm^2 obtained after graphene growth. The LEED only shows the sixfold (1 × 1) graphite diffraction spots, in agreement with micro-Raman spectroscopy (Figure S1, Supporting Information). This finding indicates the presence of only a single orientation of the graphene layers and the absence of rotational disorder and twinning domains. The absence of a (1 × 1) signature of the SiC substrate and a $(6\sqrt{3} \times 6\sqrt{3})R30°$ signature of the interface layer is due to the thick graphene multilayer, which attenuates the electron beam. The topographic atomic force microscopy (AFM) image (Figure 1b) shows a self-ordered stepped surface. The terraces are fully covered by graphene. The step direction and the terrace width are determined by the initial misorientation of the 3C-SiC substrate with respect to the crystallographic (111) plane. No pits and antiphase domain boundaries are seen.[18]

In order to investigate the stacking structure of the multilayer graphene, cross-sectional STEM experiments were performed. When the crystals are oriented along the ⟨110⟩ zone axis, only 3C-SiC(111) was resolved with atomic resolution (Figure 1c), indicating that the multilayer graphene is not oriented along this axis. In order to atomically resolve multilayer graphene, we need to orient the crystals along the ⟨112⟩ SiC zone

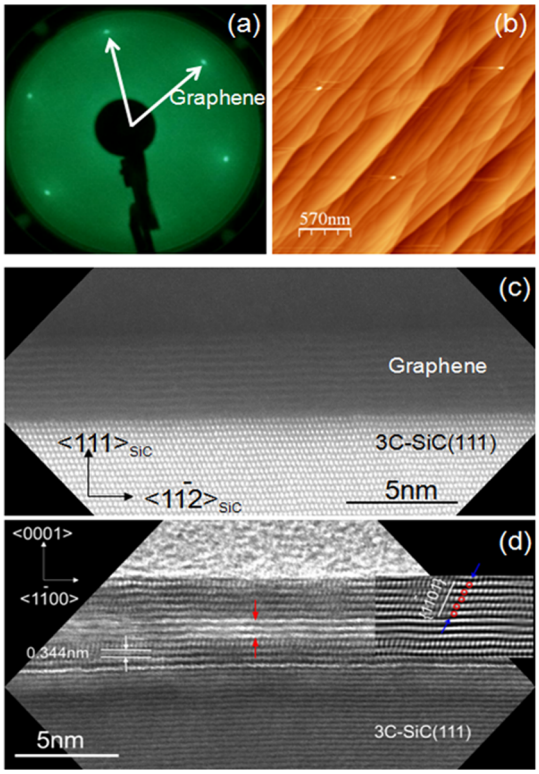

Figure 1. Morphological and electronic properties of multilayer graphene on 3C-SiC(111). (a) LEED pattern at 124 eV showing the diffraction spots due to the graphene lattice (white arrows), as well as the absence of spots of the $(6\sqrt{3} \times 6\sqrt{3})R30°$ interface layer and the (1×1) spots of the SiC substrate. (b) Typical AFM image of the multilayer graphene on cubic SiC. (c) Atomic resolution high-angle annular dark-field STEM image of the multilayer graphene cross section after focused ion beam (FIB) preparation. The 3C-SiC epilayer is exactly oriented along a $\langle 110 \rangle$ zone axis. The multilayer graphene crystal is not on an axis. (d) Atomic resolution bright-field STEM image of the multilayer graphene observed in the cross section after FIB preparation. An inverse filtered image is given at its corresponding place in the inset. The rhombohedral stacking of the multilayer graphene stacking is observed when the crystal is oriented along a $\langle 11\bar{2}0 \rangle$ zone axis.

axis. A cross-sectional atomic resolution bright-field scanning transmission electron microscope (BF-STEM) image of multilayer graphene on 3C-SiC(111) is shown in Figure 1d. Eleven graphene layers are present. The interplanar spacing for the (0003) basal plane is measured at 0.344 ± 0.001 nm, and the angle between the $\{1\bar{1}01\}$ and the (0003) basal plane is $65 \pm 1.5°$ (depending on the area on the multilayer graphene). In particular, the inverse fast Fourier transform (IFFT) image (inset in Figure 1d) shows purely rhombohedral stacking without any Bernal layers. The rhombohedral domains are about 40−50 nm, with an estimated stacking coverage of about 70% of the sample (selected area electron diffraction of the multilayer graphene is shown in Supporting Information Figure S2). We also note that a stacking fault of about three layers (twisted angle of about 2°/3°) between the topmost and bottom layers is present (inside the red arrows in Figure 1d), thus decoupling the five rhombohedral stacking layers from the bottom. This particular stacking is reproducible in several areas of the sample. The coherence length of the rhombohedral domains along the axis growth is about five/six layers. This is an important advance in the elaboration of large-area and long-sequence ABC-stacked multilayer graphene.

In order to obtain a structural and spectroscopic fingerprint showing the existence of rhombohedral multilayer graphene in our samples, we carried out STM and STS measurements at a temperature of 4.2 K, together with DFT calculations of the local density of states (LDOS) (see Methods). By measuring simultaneously the constant-current image and the differential conductance d*I*/d*V* as a function of position, we compared the topography (Figure 2a) and the maps of LDOS (Figure 2b) for a fixed voltage, $V = 100$ meV. The surface consists of 600 nm wide, atomically flat terraces that are separated by steps with a height of multiple unit cells (1−2 nm). The terrace width results from the step bunching of 3C-SiC(111) epilayers. In Figure 2b, areas of high and low differential conductance are well-identified. Transitions between homogeneous conductance domains are highlighted by a black line. We can assign the two domains to rhombohedral and Bernal stacking, as attested by the analysis of the STS data reported below. By analyzing several areas of the sample and using the LDOS map (as in Figure 2b), we estimated the coverage due to rhombohedral stacking to be 70% of the surface, in agreement with STEM measurements. The percentage of rhombohedral stacking in this case is considerably higher than rhombohedral stacking on hexagonal SiC substrates, in which it represents only 20% of the surface.[19] Remarkably, the graphene lattice uninterruptedly crosses the boundaries between the domains, as shown in Figure 2c (see Supporting Information Figure S3 for a 3D image).

The comparison between DFT calculations and spatially resolved STS d*I*/d*V* *versus* bias voltage (V_{bias}) spectra shown in Figure 2d,e permitted us to identify the Bernal or rhombohedral stacking. Indeed, while the standard V-shaped spectrum is evident in the right region of Figure 2c, a pronounced peak with a narrow width of about 30 mV (fwhm) near the Fermi energy is clearly resolved in the spectrum measured in the left region. The close agreement between STS spectra and DFT-calculated LDOS provides unambiguous proof that the stacking of the left region is rhombohedral, while that in the right region is Bernal. Moreover, as shown in Figure S5 in the Supporting Information, in the case of rhombohedral stacking, the position of the secondary peaks at ±200−300 meV and the intensity ratio between the peak at the Fermi level and of the secondary peaks vary substantially with the number of layers. Our calculations support a five-layer rhombohedral graphene flake, in agreement with results from STEM experiments.

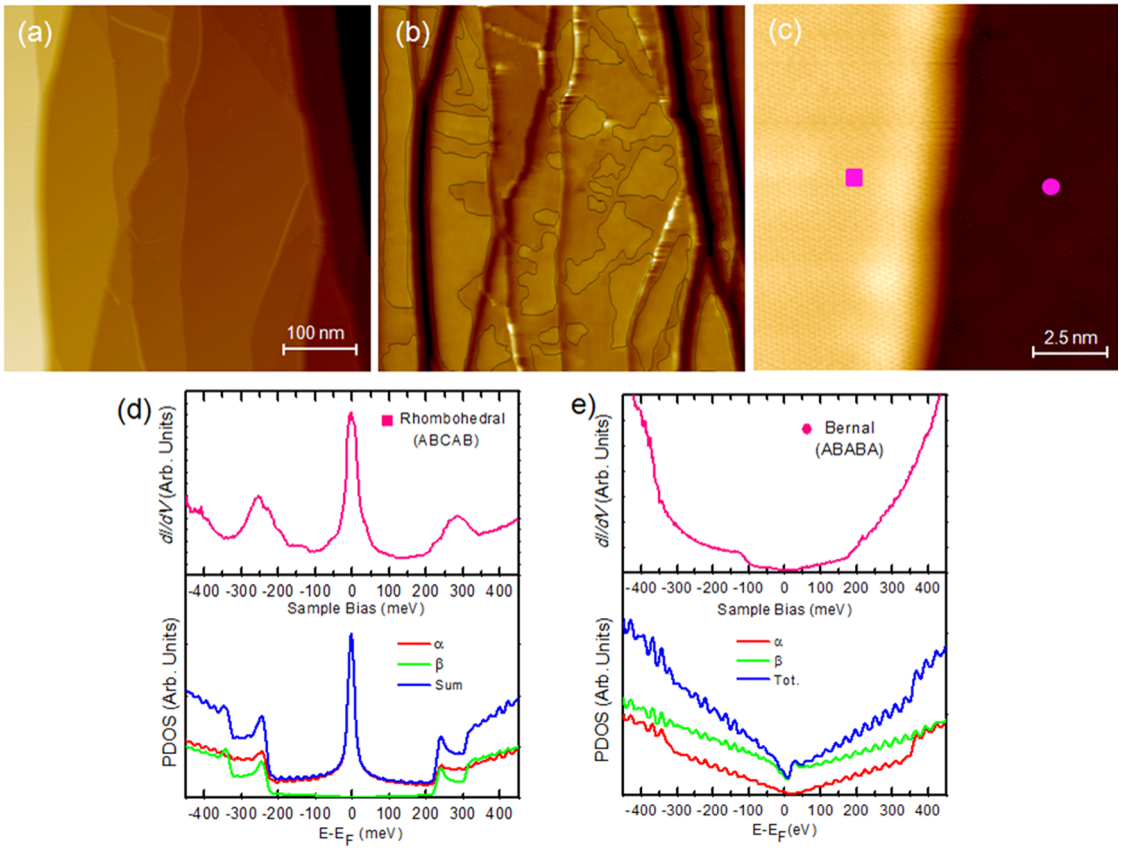

Figure 2. STM/STS studies of the transition rhombohedral/Bernal stacking of multilayer graphene (T = 4.2 K). (a) Large-scale STM topographic image (500 × 500 nm^2, 100 mV, 200 pA, color scale: 0−21 nm) showing an area of bunched steps. (b) Differential conductance dI/dV map simultaneously recorded in the same area and under the same conditions as image (a). High and low differential conductance areas correspond to rhombohedral and Bernal stacking, respectively. (c) Atomic resolution STM image of the coherence crystal at the step edges of the multilayer graphene (15 × 15 nm^2, 100 mV, 200 pA, color scale: 0−0.76 nm). (d,e) Experimental spectra of five-layer Bernal and rhombohedral stacking collected at the left and right side of panel c, respectively, *vs* theoretical STS spectra. In the theoretical spectra, we show the density of states projected on the α and β C atoms of the surface layer and the sum of these two contributions; α and β are the two sublattices of the graphene layer.

Figure 3a,b shows an STM and tunneling current image of the transition from the Bernal to the rhombohedral structure (from left to right in the figures) in the absence of a step edge. The two domains are identified by the STS measurements. There is no measurable difference in the lattice parameters of the two regions. The Fourier transform (FT) of the STM images is shown in Figure 3c: the surface exhibits clearly two ordered structures with the (1 × 1) symmetry of the graphene layer. The most intense spots are due to the Bernal and rhombohedral stacking, while the less intense spots are attributed to the "no overlap" regions which present a small strain (∼0.4%). From the FTs, it is possible to measure the spatial periodicity of 2.45 Å for both stacks.

Figure 3d is the magnified STM image of the region shown in Figure 3a, where we can appreciate the continuous transition between the local Bernal and rhombohedral stacking. The presence of two amplitudes in the surface atomic corrugations can be seen in the line scan presented in Figure 3e. The average width of this transition region is estimated to be about 4 nm, and its apparent depression is about 40 pm.[19] It is worthwhile to notice the honeycomb pattern observed in this region. A graphene lattice is composed of α and β sublattices, and this asymmetry in the surface atom electronic environment results in a three-fold symmetry six-for-three pattern in which three bright or dark features can be observed for each set of six carbon atoms. This is an uncommon observation in rhombohedral and Bernal-type stacking, where two nonequivalent sites (α and β) are probed by the STM tip in the surface primitive cell. Indeed, the honeycomb structure is regularly observed in monolayer graphene or in the case of few-layer graphene presenting either an incommensurate shift between top and bottom layers or an "AA stacking".[20] In Figure 3f, we show that the equivalence between α and β sites can be recovered also in the transition region when one of the two layers in the Bernal stacking is shifted by a fraction of a unit cell vector with respect to the other layer to recover the neighboring rhombohedral stacking.

As STEM and STM/STS are local microscopic probes, in order to judge the homogeneity of the rhombohedral

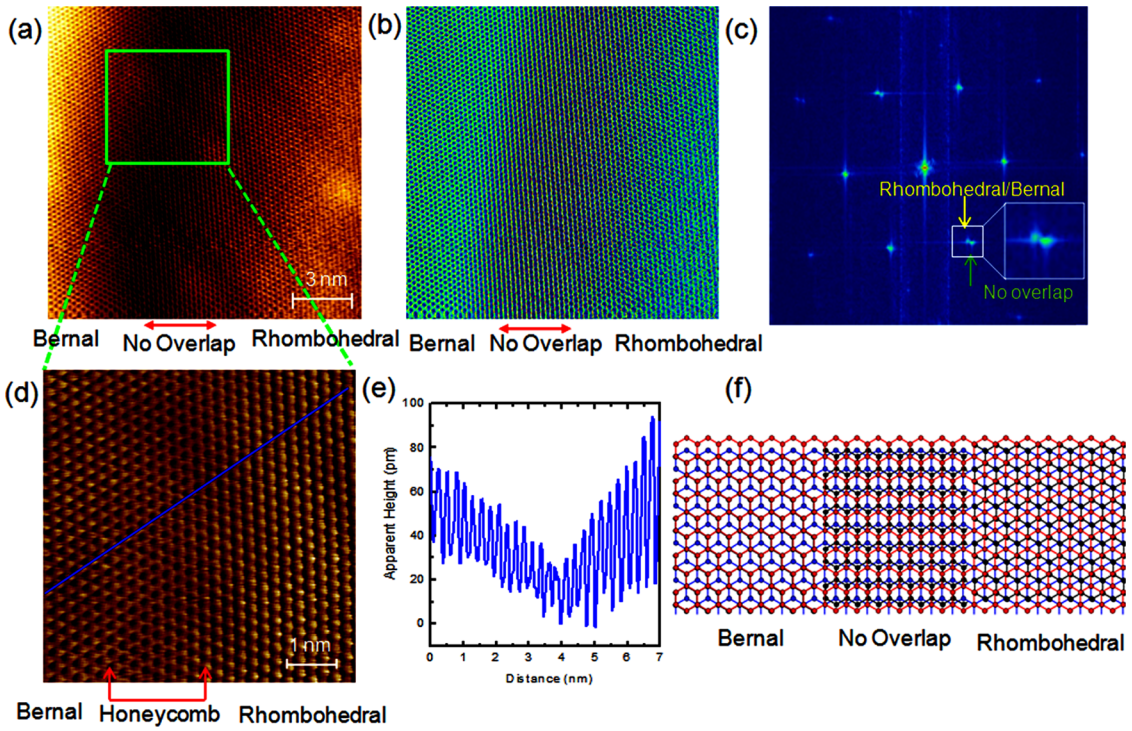

Figure 3. STM images of the rhombohedral/Bernal stacking transition of multilayer graphene at the same terraces ($T = 4.2$ K). (a,b) Large-scale (15 × 15 nm^2, 100 mV, 200 pA, color scale: 0−0.30 nm) STM topographic and STM tunneling current image of the transition between Bernal and rhombohedral stacking. (c) Fast Fourier transformation of (a) showing the periodicity of the graphene lattice as well as that of the (1 × 1) pattern induced by the no overlap transition. (d) Zoom (6 × 6 nm^2, 100 mV, 200 pA, color scale: 0−0.20 nm) of (a) showing graphite (left and right) and graphene-like (honeycomb) surface charge densities (middle). (e) Profile line showing the presence of two roughnesses at the terraces. (f) Schematic structure of the rhombohedral and Bernal stacking transition.

sample and its extension, we also performed ARPES at the APE beamline of the ELETTRA synchrotron. Figure 4a shows ARPES data taken around the K point along the ΓK direction of the first Brillouin zone for an incident photon energy of $h\nu$ = 60 eV and a probed area of approximately 50 × 100 μm^2. Although we have several (at least 11) layers of graphene, the ARPES map is different from a graphite-like band structure,[21] suggesting a decoupling of the upper layers of graphene, as shown in the STEM data (Figure 1d). Following the maximum intensity in this map at energies well below the Fermi level, a linear-shaped dispersion is observed. This agrees with the expected conical dispersion of relativistic electrons near the Dirac point. From the analysis of the energy distribution curves (EDC) shown in Figure 4b, we observe a high density of states at the Fermi level, in agreement with the occurrence of rhombohedral stacking. Near the K point, the flat band region extends by about 0.08 A^{-1}. More insight can be obtained by taking the second derivative of the ARPES spectrum, as shown in Figure 4c. Within the experimental accuracy, two mixed internal bands are observed with intersections located at 0.3 and 0.6 eV below the Fermi level. The one at 0.3 eV below has a higher intensity, and remarkably, it is not centered on the K point. By comparing with electronic structure calculations on pentalayer graphene with Bernal and rhombohedral stackings (in Figure 4d−f, we consider a pure Bernal ABABA sequence, a pure rhombohedral ABCAB sequence, and a mixed rhombohedral−Bernal ABCAC sequence), we see that the extension of the flat band at the Fermi energy and the shift from the K point of the maximum of the band at 0.3 eV is only consistent with the presence of a long rhombohedral sequence. In addition, the flat band region extends by about 0.08 A^{-1}; this value is in agreement with the theoretical flat band of ABCABC band structure. However, we do not exclude the possibility of the presence of ABCAC structure. The measured ARPES band structure is thus consistent with the occurrence of rhombohedral-type stacking in undoped multilayer graphene on 3C-SiC(111). In order to study the stability of these flat bands, we exposed the surface of multilayer graphene on 3C-SiC(111) to air for 1 year. After being annealed at 600 or 900 °C for 30 min, no oxygen traces due to eventual contaminations and/or oxidation were observed in XPS spectra (no contribution at ∼530 eV in Figure S7 Supporting Information). Interestingly, ARPES data are characterized by a band structure identical to that obtained in Figure 4d, with a flat band close to the Fermi level/Dirac points (Figure S8). In order to underline the role of the substrate, we have also studied the stacking of the same thickness of graphene layers on 4H-SiC(0001).

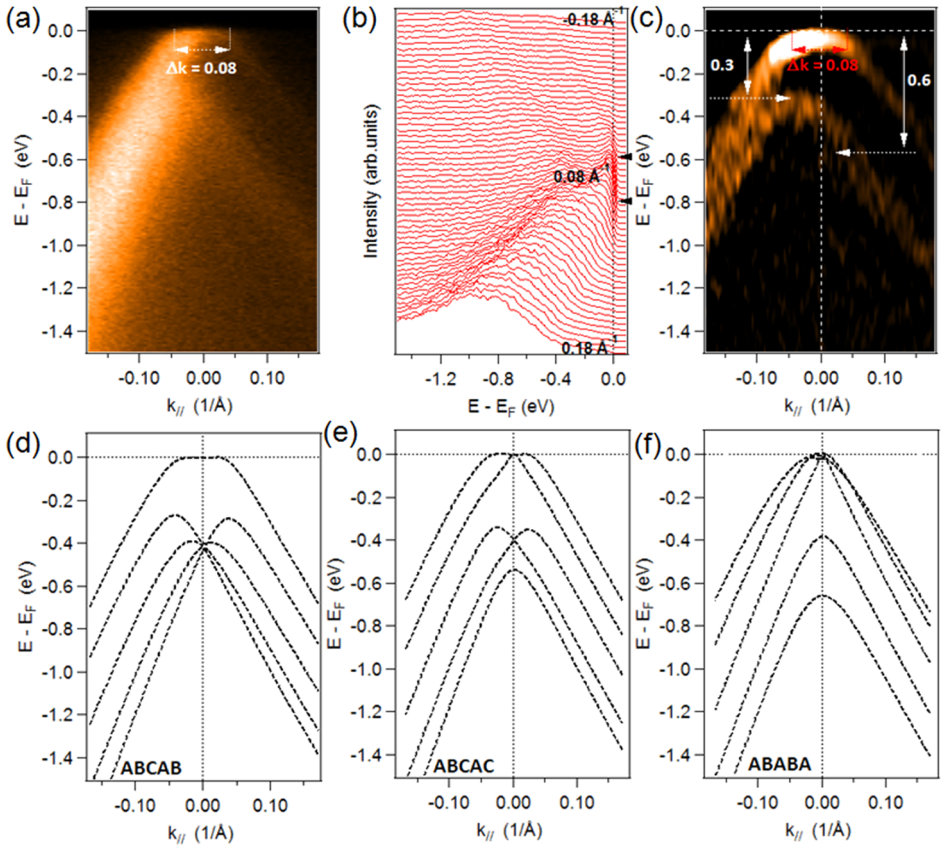

Figure 4. Electronic structure of multilayer graphene. (a) Dispersion of the π bands measured by ARPES. The spectra are measured with a photon energy of 60 eV and with scans oriented along the ΓK direction of the graphene Brillouin zone. (b) EDC of (a), showing the presence of a flat band. (c) Second derivative of the intensity ARPES data along the ΓK direction of the multilayer graphene. (d–f) Theoretical calculation of five layers with pure rhombohedral ABCAB, mixed rhombohedral–Bernal ABCAC, and pure Bernal ABABA sequence.

Figure S9a,b shows XPS and ARPES data. The XPS spectrum performed on a wide energy range is identical to that of multilayer graphene on 3C-SiC(111) (Figure S7). The ARPES map taken around the K point along the ΓK direction of the first Brillouin zone is similar to a graphitic-like band structure without the presence of the flat band at the Fermi Level. This result confirms the presence of a high-density Bernal stacking graphene on 4H-SiC(0001) with respect to multilayer graphene on 3C-SiC(111), confirming that the substrate also has an important role in the stacking order.

CONCLUSIONS

In summary, we have demonstrated that high-quality multilayer graphene can be obtained on cubic SiC/off-axis 6H-SiC(0001) substrates. The homogeneity, large area, and high quality of the sample are confirmed by AFM imaging. The STEM data suggest that, when grown on 3C-SiC(111) substrates, graphene exhibits a large amount of rhombohedral stacking (~70%), much more marked than in natural graphite. Moreover, the sequence of rhombohedral stacking is up to five layers, well beyond the ABC trilayer previously obtained on cubic 3C-SiC(111) substrates.[17] STM experiments confirm the lateral and vertical extent of the rhombohedral stacking in our samples. Nicely, a peculiar LDOS, characterized by an intense and narrow peak close to E_F, is probed by STS experiments. Finally, we have directly visualized, by ARPES measurements, the electron band dispersion spectra of rhombohedral-stacked multilayers and shown that they correlate well with the DFT calculations and the STS measurements. The flat band observed close to E_F contributes to the pronounced peak in the tunneling density of states, and it is a genuine consequence of the rhombohedral stacking.

METHODS

Sample Preparation. The 3C-SiC(111) seed was elaborated in two steps: first a 2 μm thick twin-free 3C-SiC(111)[22] layer was grown by a vapor–liquid–solid mechanism on 2° off-oriented (toward [11–20]), Si face 6H-SiC(0001) commercial wafer. Then this 3C-SiC layer was thickened to 12 μm by chemical vapor deposition at 1600 °C; see ref 23 for more details. The 3C-SiC was the heated to 1600 °C in an Ar atmosphere (800 mbar) for 10 min in order to obtain multilayer graphene.[24] The sample

was then cooled to room temperature and transferred *ex situ* from the growth chamber to undergo XPS/ARPES and STM/STS measurements. Before each measurement, samples were annealed at 600 °C for 30 min to remove surface contaminations.

Characterization: LEED/AFM/STM/STS/XPS/ARPES. STM/STS measurements were carried out using an Omicron ultrahigh vacuum low-temperature scanning tunneling microscope (UHV-LT-STM). STM/STS measurements were acquired at 4.2 K in the constant current mode for different bias voltages V applied to the sample. For the STS measurements, performed at $T = 4.2$ K, the $I(V)$ characteristics were acquired while the feedback loop was inactive, and the differential conductivity dI/dV (V, x, y), proportional to the LDOS, was measured directly by using a lock-in technique. For this purpose, a small AC modulation voltage V_{mod} was added to V ($V_{mod,p\text{-}p} = 10$ mV, $f_{mod} = 973$ Hz), and the signal dI/dV was detected using a lock-in amplifier in order to determine the differential conductivity dI/dV_{mod}. ARPES measurements were carried out at APE beamline[25] (ELETTRA Italian synchrotron facility). The photon source was an APPLE II-type quasi-periodic undulator (energy range 10−100 eV) set to deliver linearly polarized light. The light was monochromatized by variable spacing gratings and then focused on the sample into a spot size 50 × 100 ($H \times V$) μm^2. Incoming photons impinged on the sample at 45° from its normal. The emitted photoelectrons were detected by a SES-2002 hemispherical analyzer with an acceptance angle of ±7° operated with an angular resolution of 0.2°. The experiment was carried out at liquid nitrogen temperature (~77 K) with a total energy resolution of 15 meV. The photon energy ($h\nu = 60$ eV) and sample orientation were set in order to explore the k space region around the K point in the ΓK direction of the Brillouin zone. XPS/ARPES experiments after 1 year were carried out at TEMPO beamline[26] (SOLEIL French synchrotron facility) at low temperature (~120 K). The photon source was a HU80 Apple II undulator set to deliver linearly polarized light. The photon energy was selected using a high-resolution plane grating monochromator, with a resolving power $E/\Delta E$ that can reach 15 000 on the whole energy range (45−1500 eV). The end-station chamber (base pressure = 10^{-10} mbar) was equipped with a modified 200 nm hemispheric electron analyzer (Scienta 200) equipped with a delay line detector.[27] For ARPES measurements, the photon energy ($h\nu = 60$ eV) and sample orientation were set in order to explore the k space region around the K point in the ΓK direction of the Brillouin zone. The photon beam impinged on the sample at an angle of 43°, and photoelectrons were detected around the sample surface normal with an angular acceptance of 6°. The spot size was 100 × 40 ($H \times V$) μm^2.

DFT Calculation. The electronic structure calculations were performed using the QUANTUM-ESPRESSO[28] code. We used the local density approximation and norm-conserving pseudopotentials and a PW energy cutoff of 65 Ry. For the electronic integration in the self-consistent calculation, we used a 256^2 electron-momentum mesh with a 1 meV Gaussian smearing. We computed the local DOS using a denser 512^2 electron-momentum grid. In all figures of the paper, the DFT band energy was rescaled by a 1.18 multiplicative factor to correct for the DFT underestimation of the Fermi velocity.[29]

Conflict of Interest: The authors declare no competing financial interest.

Acknowledgment. This work was supported by ANR SUPERTRAMP, ANR NANOTMD grants, the EU Graphene Flagship and Labex Nanosaclay. The authors thank Ivana Vobornik and Giancarlo Panaccione of the APE beamline, and ELETTRA Synchrotron facility for their excellent technical support during ARPES measurements.

Supporting Information Available: Raman spectroscopy spectra of multilayer graphene on 3C-SiC(111) (Figure S1), TEM/STEM analysis on multilayer graphene on 3C-SiC(111) substrate (Figure S2), 3D image of Figure 2c (Figure S3), STS spectra at different areas of the sample and local density of states for different numbers of layers (Figure S4 and Figure S5), calculated band structure for different numbers of layers (Figure S6), XPS and ARPES spectroscopy of the sample after 1 year (Figure S7 and Figure S8), and XPS and ARPES spectroscopy of multilayer graphene on 4H-SiC(0001) substrate (Figure S9). This material is available free of charge *via* the Internet at http://pubs.acs.org.

REFERENCES AND NOTES

1. Olsen, R.; van Gelderen, R.; Smith, C. Ferromagnetism in ABC-Stacked Trilayer Graphene. *Phys. Rev. B* **2013**, *87*, 115414.
2. Kopnin, N.; Ijäs, M.; Harju, A.; Heikkilä, T. High-Temperature Surface Superconductivity in Rhombohedral Graphite. *Phys. Rev. B* **2013**, *87*, 140503(R).
3. Kopnin, N. B.; Heikkilä, T. T.; Volovik, G. E. High-Temperature Surface Superconductivity in Topological Flat-Band Systems. *Phys. Rev. B* **2011**, *83*, 220503(R).
4. Norimatsu, W.; Kusunoki, M. Selective Formation of ABC-Stacked Graphene Layers on SiC(0001). *Phys. Rev. B* **2010**, *81*, 161410(R).
5. Lin, Q.; Li, T.; Liu, Z.; Song, Y.; He, L.; Hu, Z.; Guo, Q.; Ye, H. High-Resolution TEM Observations of Isolated Rhombohedral Crystallites in Graphite Blocks. *Carbon* **2012**, *50*, 2369–2371.
6. Warner, J. H.; Mukai, M.; Kirkland, A. I. Atomic Structure of ABC Rhombohedral Stacked Trilayer Graphene. *ACS Nano* **2012**, *6*, 5680–5686.
7. Yankowitz, M.; Wang, J. I.; Birdwell, A. G.; Chen, Y.; Watanabe, K.; Taniguchi, T.; Jacquod, P.; San-Jose, P.; Jarillo-Herrero, P.; Leroy, B. J. Electric Field Control of Soliton Motion and Stacking in Trilayer Graphene. *Nat. Mater.* **2014**, *13*, 786–789.
8. Ouerghi, A.; Kahouli, A.; Lucot, D.; Portail, M.; Travers, L.; Gierak, J.; Penuelas, J.; Jegou, P.; Shukla, A.; Zielinski, M. Epitaxial Graphene on Cubic SiC (111)/Si (111) Substrate. *Appl. Phys. Lett.* **2010**, *96*, 191910–191913.
9. Ouerghi, A.; Belkhou, R.; Marangolo, M.; Silly, M. G.; El Moussaoui, S.; Eddrief, M.; Largeau, L.; Portail, M.; Sirotti, F. Structural Coherency of Epitaxial Graphene on 3C-SiC-(111) Epilayers on Si(111). *Appl. Phys. Lett.* **2010**, *97*, 161905.
10. Ouerghi, A.; Marangolo, M.; Belkhou, R.; El Moussaoui, S.; Silly, M. G.; Eddrief, M.; Largeau, L.; Portail, M.; Fain, B.; Sirotti, F. Epitaxial Graphene on 3C-SiC(111) Pseudosubstrate: Structural and Electronic Properties. *Phys. Rev. B* **2010**, *82*, 125445.
11. Fukidome, H.; Takahashi, R.; Abe, S.; Imaizumi, K.; Handa, H.; Kang, H.-C.; Karasawa, H.; Suemitsu, T.; Otsuji, T.; Enta, Y.; et al. Control of Epitaxy of Graphene by Crystallographic Orientation of a Si Substrate toward Device Applications. *J. Mater. Chem.* **2011**, *21*, 17242.
12. Fukidome, H.; Abe, S.; Takahashi, R.; Imaizumi, K.; Inomata, S.; Handa, H.; Saito, E.; Enta, Y.; Yoshigoe, A.; Teraoka, Y.; et al. Controls over Structural and Electronic Properties of Epitaxial Graphene on Silicon Using Surface Termination of 3C-SiC-(111)/Si. *Appl. Phys. Express* **2011**, *4*, 115104.
13. Suemitsu, M.; Jiao, S.; Fukidome, H.; Tateno, Y.; Makabe, I.; Nakabayashi, T. Epitaxial Graphene Formation on 3C-SiC/Si Thin Films. *J. Phys. D: Appl. Phys.* **2014**, *47*, 094016.
14. Gupta, B.; Notarianni, M.; Mishra, N.; Shafiei, M.; Iacopi, F.; Motta, N. Evolution of Epitaxial Graphene Layers on 3C SiC/Si(111) as a Function of Annealing Temperature in UHV. *Carbon* **2014**, *68*, 563–572.
15. Cordier, Y.; Frayssinet, E.; Portail, M.; Zielinski, M.; Chassagne, T.; Korytov, M.; Courville, A.; Roy, S.; Nemoz, M.; Chmielowska, M.; et al. Influence of 3C-SiC/Si (111) Template Properties on the Strain Relaxation in Thick GaN Films. *J. Cryst. Growth* **2014**, *398*, 23–32.
16. Coletti, C.; Emtsev, K. V.; Zakharov, A. A.; Ouisse, T.; Chaussende, D.; Starke, U. Large Area Quasi-Free Standing Monolayer Graphene on 3C-SiC(111). *Appl. Phys. Lett.* **2011**, *99*, 081904.
17. Coletti, C.; Forti, S.; Principi, A.; Emtsev, K. V.; Zakharov, A. A.; Daniels, K. M.; Daas, B. K.; Chandrashekhar, M. V. S.; Ouisse, T.; Chaussende, D.; et al. Revealing the Electronic Band Structure of Trilayer Graphene on SiC: An Angle-Resolved Photoemission Study. *Phys. Rev. B* **2013**, *88*, 155439-6.
18. Velez-Fort, E.; Silly, M. G.; Belkhou, R.; Shukla, A.; Sirotti, F.; Ouerghi, A. Edge State in Epitaxial Nanographene on 3C-SiC(100)/Si(100) Substrate. *Appl. Phys. Lett.* **2013**, *103*, 083101.

19. Lalmi, B.; Girard, J. C.; Pallecchi, E.; Silly, M.; David, C.; Latil, S.; Sirotti, F.; Ouerghi, A. Flower-Shaped Domains and Wrinkles in Trilayer Epitaxial Graphene on Silicon Carbide. *Sci. Rep.* **2014**, *4*, 4066.
20. Xu, P.; Yang, Y.; Qi, D.; Barber, S. D.; Ackerman, M. L.; Schoelz, J. K.; Bothwell, T. B.; Barraza-Lopez, S.; Bellaiche, L.; Thibado, P. M. A Pathway between Bernal and Rhombohedral Stacked Graphene Layers with Scanning Tunneling Microscopy. *Appl. Phys. Lett.* **2012**, *100*, 201601.
21. Zhou, S. Y.; Gweon, G.-H.; Graf, J.; Fedorov, A. V.; Spataru, C. D.; Diehl, R. D.; Kopelevich, Y.; Lee, D.-H.; Louie, S. G.; Lanzara, A. First Direct Observation of Dirac Fermions in Graphite. *Nat. Phys.* **2006**, *2*, 595–599.
22. Ouerghi, A.; Balan, A.; Castelli, C.; Picher, M.; Belkhou, R.; Eddrief, M.; Silly, M. G.; Marangolo, M.; Shukla, A. Epitaxial Graphene on Single Domain 3C-SiC (100) Thin Films Grown on Off-Axis. *Appl. Phys. Lett.* **2012**, *101*, 021603.
23. Lorenzzi, J.; Esteve, R.; Jegenyes, N.; Reshanov, S. A.; Schöner, A.; Ferro, G. MOS Capacitors Fabricated on 3C-SiC(111) Layers Grown on 6H-SiC(0001). *J. Electrochem. Soc.* **2011**, *158*, H630.
24. Pallecchi, E.; Lafont, F.; Cavaliere, V.; Schopfer, F.; Mailly, D.; Poirier, W.; Ouerghi, A. High Electron Mobility in Epitaxial Graphene on 4H-SiC(0001) *via* Post-Growth Annealing under Hydrogen. *Sci. Rep.* **2014**, *4*, 4558.
25. Panaccione, G.; Vobornik, I.; Fujii, J.; Krizmancic, D.; Annese, E.; Giovanelli, L.; Maccherozzi, F.; Salvador, F.; De Luisa, A.; Benedetti, D.; et al. Advanced Photoelectric Effect Experiment Beamline at Elettra: A Surface Science Laboratory Coupled with Synchrotron Radiation. *Rev. Sci. Instrum.* **2009**, *80*, 043105.
26. Polack, F.; Silly, M.; Chauvet, C.; Lagarde, B.; Bergeard, N.; Izquierdo, M.; Chubar, O.; Krizmancic, D.; Ribbens, M.; Duval, J.-P.; et al. TEMPO: A New Insertion Device Beamline at SOLEIL for Time Resolved Photoelectron Spectroscopy Experiments on Solids and Interfaces. *AIP Conf. Proc.* **2010**, *1234*, 185–188.
27. Bergeard, N.; Silly, M. G.; Krizmancic, D.; Chauvet, C.; Guzzo, M.; Ricaud, J. P.; Izquierdo, M.; Stebel, L.; Pittana, P.; Sergo, R.; et al. Time-Resolved Photoelectron Spectroscopy Using Synchrotron Radiation Time Structure. *J. Synchrotron Radiat.* **2011**, *18*, 245–250.
28. Giannozzi, P.; Baroni, S.; Bonini, N.; Calandra, M.; Car, R.; Cavazzoni, C.; Ceresoli, D.; Chiarotti, G. L.; Cococcioni, M.; Dabo, I.; et al. QUANTUM ESPRESSO: A Modular and Open-Source Software Project for Quantum Simulations of Materials. *J. Phys.: Condens. Matter* **2009**, *21*, 395502.
29. Park, C.-H.; Giustino, F.; Cohen, M.; Louie, S. Velocity Renormalization and Carrier Lifetime in Graphene from the Electron−Phonon Interaction. *Phys. Rev. Lett.* **2007**, *99*, 086804.